7th Australian Conference on Laser Diagnostics in Fluid Mechanics and Combustion
Melbourne, Australia
9-11 December 2015

The application of laser diagnostics to cycling aerodynamics T. N.

T.N. Crouch[1], **N. Barry**[1], **J.A Venning**[1], **D. Burton**[1], **M. C. Thompson**[1], and **J. Sheridan**[1]

[1] Department of Mechanical and Aerospace Engineering
Monash University, Clayton, Victoria, Australia

Abstract

To improve the aerodynamic performance of cyclists, detailed information of the flow field is required around these highly three-dimensional bluff-body geometries. Using traditional measurement techniques with cyclists in a wind tunnel, it is often difficult or impractical to acquire detailed flow field surveys. In this paper two examples are discussed where high-resolution Particle Image Velocimetry has been undertaken in a water channel to investigate the wake dynamics of a single pedalling cyclist and the flow between multiple cyclists. These areas have previously been difficult to measure experimentally using intrusive measurement techniques. The first example provides a comparison of the phase-averaged wake of a 1:4.5 scale pedalling cyclist/bicycle combination in the water channel and that of a full-scale cyclist mannequin of similar geometry and position in a wind tunnel. The second example shows an application of PIV to measure the flow field between two drafting cyclists. Good agreement is observed between the large-scale wake of the scale model and full-scale mannequin despite an order-of-magnitude difference in Reynolds number. The drafting model shows that for spacings greater than a bike length, the trailing rider has negligible effect on the wake of the upstream rider.

Introduction

Aerodynamic efficiency is critical for success in competitive cycling. At elite speeds on relatively flat surfaces, as much as 90% of the total energy expended by a cyclist is used to overcome drag [1, 2]. Furthermore, the power required, P_{Aero}, scales with the third power of the freestream velocity

$$P_{Aero} = 0.5\rho U_\infty^3 C_D A, \qquad (1)$$

where ρ is the air density, C_D is the drag coefficient and A is the projected frontal area. At racing speeds (typically >10 m/s) this term greatly dominates mechanical and frictional resistance acting on the cyclist/bicycle system.

Cyclists competing in individual events can therefore reduce aerodynamic resistance by either lowering their projected frontal area or reducing their drag coefficient. Rider posture has been shown to have the largest influence on these variables, while equipment selection and design typically have only secondary effects [1, 3, 4]. As a cyclist's frontal area and drag coefficient are influenced simultaneously when optimising position and equipment, predicting the change in aerodynamic drag is often difficult, due to the non-linear relationship between A and C_D. A better understanding of the three-dimensional flow field around a cyclist, and the primary mechanisms responsible for drag, leads to better informed decisions to attempt to reduce drag and may potentially lead to new techniques for aerodynamic optimisation.

Experimental studies by Crouch *et al.* [5] have provided insight into the dominant fluid mechanisms influencing cycling aerodynamics through characterising the large-scale flow structures that develop from the cyclist and extend into the wake. Wind tunnel studies mapped the time-averaged wake flow of a full-

scale mannequin for a range of static leg positions over the full 360° crank cycle. Large changes in flow structure and aerodynamic drag, which varied by 20%, were observed. The wake flow was generally classified into two regimes: symmetric and asymmetric, which correlate with low and high drag states, respectively. The low drag symmetrical state occurred for crank angles with the upper legs approximately horizontal. The high-drag asymmetrical state occurs when one leg is raised and the other extended. For such leg positions, the wake is dominated by a strong counter-rotating vortex pair that originates from the cyclist's hips. Similar wake flow structures were also observed in numerical models by Griffith *et al.* [6].

Whilst cycling is often considered an individual sport, many cycling events involve athletes riding in teams or groups in close proximity to one another. Cyclists have understood anecdotally that following in the wake of another cyclist (drafting) offers a significant performance advantage. It has been shown that drafting can reduce the trailing rider's drag up to 49% and that of the leading rider by 5%, and that these effects degrade with separation distance [7, 4, 8]. An understanding of how the identified wake changes when cyclists are in close proximity is important in identifying the flow mechanisms responsible for the large reduction in drag and to further optimise interaction effects. Furthermore, the study of cycling may provide useful insight into bluff body flows from other complex and dynamic geometries.

The flow past a cyclist represents a challenging bluff-body flow problem, as it has a large and dynamic geometry variation resulting from the moving legs, in addition to the intrinsic complex geometry. This results in a complex, time-varying wake. Such a complex flow is difficult and time-consuming to capture and characterise at full scale in a wind tunnel using point measurement techniques. By comparison, laser diagnostic tools such as Particle Image Velocimetry (PIV) allow high-resolution flow field capture. To further our understanding of the flow around a cyclist, reduced-scale models were constructed for PIV measurements suitable for a water channel. This represents a novel technique that has the potential for far higher resolution mapping of the flow field. The use of PIV with scale models was also employed for drafting cyclists. In addition to high resolution field data, PIV also provides non-intrusive mapping between cyclists.

Experimental Method

Figure 1 (a) and (b) show the full-scale wind-tunnel mannequin and the 1:4.5 scale water-channel model respectively. Two smaller 1:7 scale models were used for the tandem cyclist water-channel experiments. The full-scale and scaled models are both depicted in the 15° leg position, which is defined through the crank angle θ. The zero-degree leg position corresponds to horizontally aligned cranks with the left leg in the downstream position. Although minor design changes have been made to the scale model, the major geometric features and dimensions have been scaled directly from the full-scale mannequin geometry detailed in Crouch *et al.* [5]. The models are based on mean geometric measurements made from experienced road cyclists, while holding a time-trial position. Features such as the head
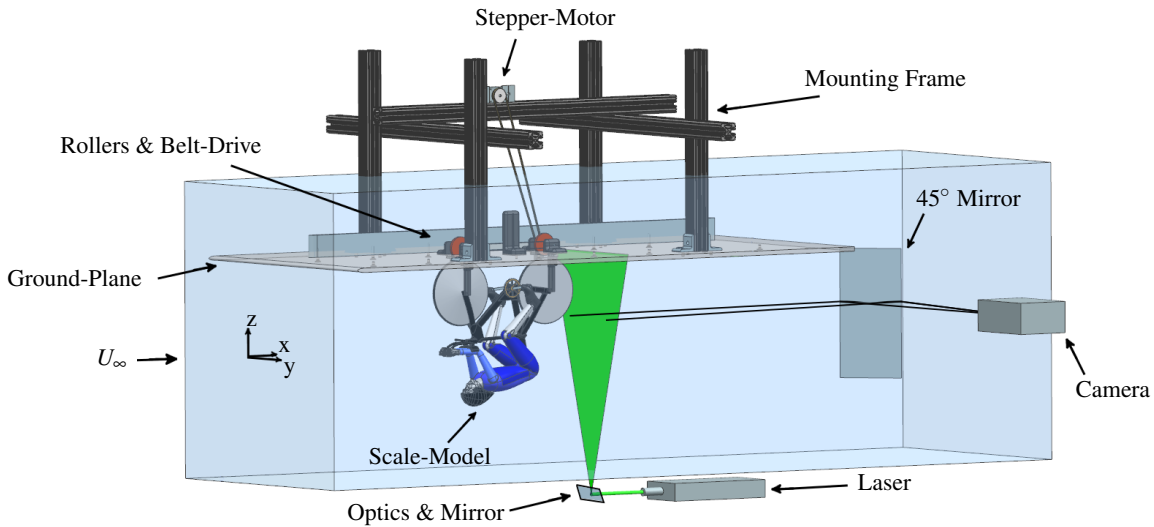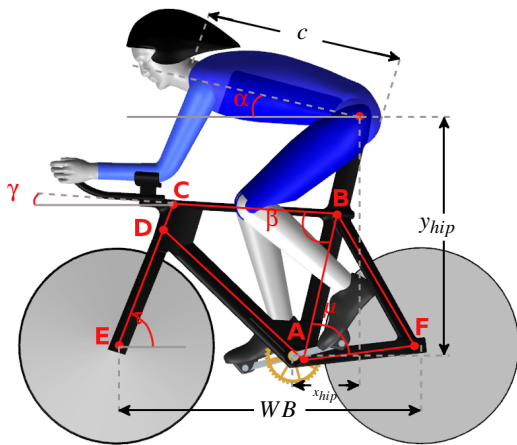
Figure 2: Schematic showing mannequin and bicycle placement in the water tunnel. Positioning of the PIV laser and camera are shown, together with the ground plane and driving mechanism of the wheels.

(a) Wind tunnel full-scale model.

(b) Water channel 1:4.5 scale-model.

Figure 1: Wind tunnel full-scale model.

and helmet are based on high-resolution scanned data.

The major difference between the scaled and full-scale models is the bicycle frame and wheel geometry. The bike frame used

in the wind tunnel studies is now outdated and was first released over 10 years ago. The simplified scale-model bicycle is based on the geometry of current *Time-Trial* (TT) bicycles from leading manufacturers and the wheels have been modelled as flat disks instead of open spoke wheels.

Particle Image Velocimetry wake measurements with the scale models were undertaken in the $0.6 \times 0.8 \times 4.0$ m working section of the Fluids Laboratory for Aeronautical and Industrial Research (FLAIR) free-surface water channel. The freestream test speed was 0.4 m/s, which corresponds to a Reynolds number of 5.7×10^4 for the 1:4.5 scale model and 3.3×10^4 for the 1:7 scale model, both based on the torso chord length c. (Note that the Reynolds number of the full-scale wind-tunnel tests compared in this study was 6.9×10^5). At this freestream velocity the test section turbulence intensity, I_u, is $< 0.5\%$ and the flow uniformity is better than $\pm 1\%$.

Figure 2 depicts the 1:4.5 scale-model setup in the water channel. The model was rigidly mounted upside down onto a ground plane via struts attached either side of the front and rear wheel axles. The ground plane extended 2WB (wheel bases) upstream and 2.5WB downstream of the leading and trailing edges of the model, respectively. The cross-sections of the struts were symmetrical airfoil profiles and, apart from providing stability, allowed positioning of the rubber front and rear tyres on the friction-drive mechanism.

The drive consisted of an electric micro-stepper-motor (50,800 steps/rev) located above the water surface that powered rollers underneath each wheel, and was connected via a 1:1 timing-belt drive system. As the wheels were made to rotate, the legs would be driven around the crank cycle through the 1:4.44 fixed gear chain and sprocket bicycle drivetrain. For all dynamic tests the legs were made to rotate at a cycling frequency f of 0.19 Hz (11.5 RPM). At this cycling cadence and gearing the wheel ground speed matched the water channel freestream velocity. This also corresponds to a reduced pedalling frequency of $k = 0.11$, which matched the conditions of the full-scale wind-tunnel tests performed at elite-level racing speeds and cadences (16 m/s at 100 RPM). The reduced frequency k, is defined as the ratio of the leg speed around the crank to the forward
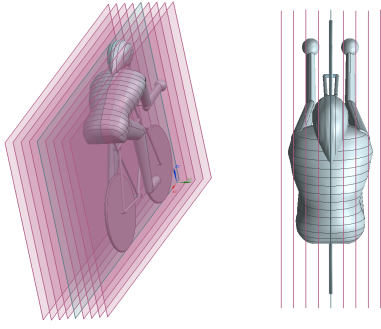
Figure 3: Series of *XZ* cross-sectional planes. Velocity field data in these planes was interpolated to capture flow information in spanwise cross sections between the two models.

riding velocity U_∞:

$$k = \frac{2\pi r f}{U_\infty}, \qquad (2)$$

where r is the crank length.

PIV vector fields were obtained in a plane normal to the freestream flow one torso length, $x/c = 1$, downstream of the rear of the model rider. The flow was seeded using Vestosint spherical particles (Vestosint, Germany) with a mean size and density of 20 μm and 1.106 g/cm^3, respectively. The particles were illuminated by a light sheet generated from two Minilite II Continuum lasers (New Wave Research Inc.,USA), in combination with a series of optical components to direct the beam and form the planar light sheet. Using a mirror positioned at 45° to the mean flow downstream of the model, a PCO.4000 CCD camera fitted with a 105 mm lens, was used to record image pairs of the spanwise planes. The resulting 2160×4008 (effective area) image pairs were analysed using in-house software (Fouras *et al.* [9]) based on a window size of 32 by 32 pixels with 75% overlap. With each pixel representing an area of 85.6×85.6 μm this resulted in a 267×498 velocity vector field, evenly spaced at 0.7 mm intervals. Phase-averaged velocity fields were determined for a number of leg positions around the crank cycle from PIV data binned into $\pm 10°$ regions. Phase-averaged velocity fields are the result of 222 image pairs recorded in each bin. The uncertainty of the velocity vectors associated with the variability of binned data was 2% U_∞ at a 95% confidence level. Due to the time taken for vortex structures to convect downstream from where they originate on the mannequin's surface to the measurement plane, the crank angle at which the phase-averaged results are depicted have been offset using the methods outlined by Crouch *et al.* [10] to correct for this lag.

For the drafting tests, two 1:7 scale models were arranged in a tandem formation, in-line and parallel to the flow direction. Two separation distances were tested: at a minimum practical separation, representing 150mm at full scale (Spacing 1), and at one bicycle length downstream of the leader (Spacing 2). To investigate flow between the leading and trailing riders a composite technique was required, as the presence of the cyclists blocks a critical region of the imaging plane from camera view. To overcome this, a series of *XZ* planes were captured at 10 mm intervals (0.1c) laterally either side of the centreline as shown in figure 3. These were focussed on the region between the leading and trailing cyclists. From these measurements, PIV data was interpolated (linear) laterally between planes to generate spanwise cross sections of the streamwise velocity component between the models.
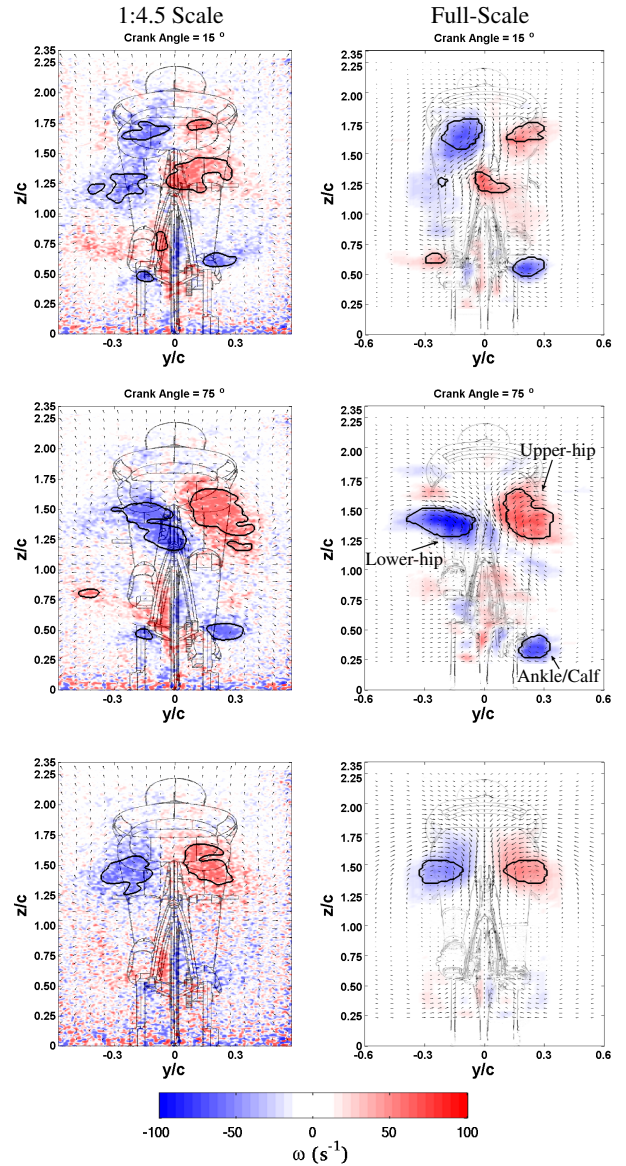
Results and Discussion

Figure 4: The left and right columns show the 1:4.5 scale and full-scale vorticity fields respectively, with respect to the spatial coordinates non-dimensionalised by the torso chord length c. The top two rows show contours of the phase-averaged streamwise vorticity fields (associated with low and high drag leg positions), with in-plane velocity vectors overlaid. The bottom row shows contours of the randomly sampled time-averaged streamwise vorticity fields with in-plane velocity vectors overlaid. Solid lines show vortices identified using the swirling strength criterion.

Pedalling Cyclist Wake Structure

Compared in the top two rows of figure 4 are contours of the phased-averaged ($k = 0.11$) streamwise vorticity fields for both the scaled model (water tunnel) and full-scale model (wind tunnel) [10] at the low (15°) and high (75°) drag leg positions in the first half of the crank cycle. To highlight the major flow structures for each flow regime, streamwise vortices have been identified using the swirling strength criterion of Zhou *et al.* [11]. Despite differences in the geometry of the two rider/bicycle models, and an order of magnitude separation of the Reynolds number, there is good agreement between the two sets of results. The characteristic symmetrical and asymmetrical flow
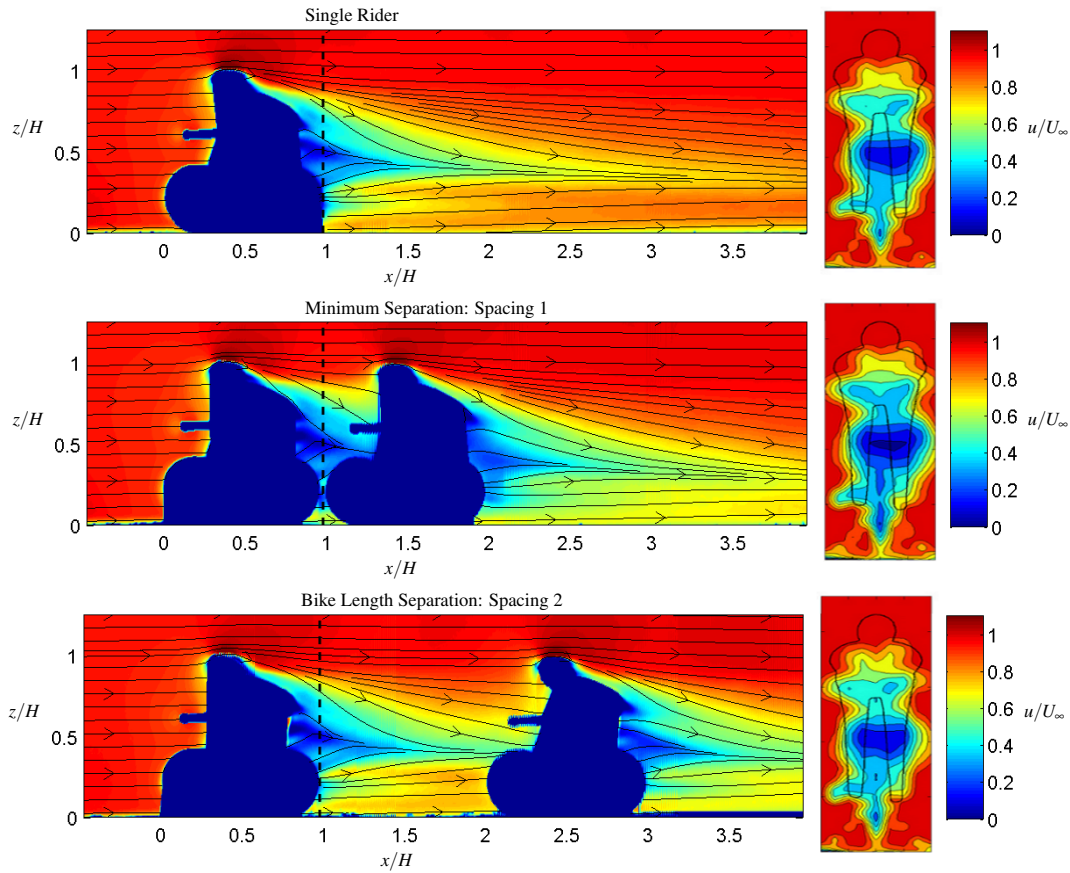
Figure 5: Left: Contours of the streamwise velocity component at the centre plane, and right: in a cross-section perpendicular to the mean flow direction immediately downstream of the trailing edge of the rear wheel of the leading rider.

states that occur over the crank cycle, as defined by Crouch *et al.* [5], are evident in both wind and water tunnel derived images for the $15°$ and $75°$ positions depicted.

The dominant and most consistent wake features are the upper and lower hip vortices, named according to where they originate on the rider [5], which form a large streamwise counter-rotating vortex pair in the wake for the $75°$ asymmetrical leg position. This was also observed for phase-averaged measurements made in the second half of the crank cycle. Excellent mirror symmetry about the centre plane is observed when comparing phase-averaged results for opposite leg positions $180°$ out of phase. A smaller well-defined vortex is also observed in the wake of the ankle/calf of the straightened leg. These large-scale and well-defined flow structures compare very well between the water-channel and wind-tunnel studies, and show good consistency in their location, size, irregular shape and strength. For a regular cycling cadence the legs and flow is predominantly in an asymmetrical state, and therefore this constitutes the majority of wake state over the crank cycle.

The persistence of the large-scale hip vortices in a time-average sense is illustrated in the bottom row of figure 4. This shows the time-averaged vorticity field over the full $360°$ rotation of the crank cycle. The streamwise vortices that originate behind the hips are clearly evident in the time-averaged dynamic leg wake. For the water-channel flow field derived from PIV measurements sampled at 12 Hz (not harmonic with the pedalling frequency), the symmetry in the flow field across the centre plane reflects the flow symmetry that was observed for opposite leg positions.

For the symmetrical $15°$ leg position a reasonable comparison is also observed between data sets. For crank angles close to the horizontal, the hip-vortices are significantly reduced in size and strength. Coherent streamwise vortices of opposite sign are also identified in the wake of both left and right ankles/calves for both water-channel and wind-tunnel results. The comparison between both scaled and full-scale results are not as strong for leg positions associated with the symmetrical flow state compared to those for the asymmetrical flow state. This may partially result from differences in the bin size used to obtain the phase-averaged flow fields. The wind-tunnel results used a much smaller bin size in the phase-averaging process compared to the water channel experiments ($6°$ compared to $20°$) [5]. In particular this would be expected to influence phase-averaged velocity fields where there is a rapid change of the flow structure over a small rotation of the crank. This behaviour is observed when the flow transitions from the symmetric to the asymmetric flow state. Despite these differences a reduction in the size and strength of the large-scale wake structures is found, and is consistent with what one would expect from the low-drag flow regime.

Drafting Cyclist Flow Field

Investigating the gap flow in between drafting cyclists is another case that presents useful application of laser diagnostic techniques. Figure 5 compares PIV time-averaged flow fields for tandem models positioned in Spacing 1 and 2 with the flow field of a single rider model in a horizontal crank position. The streamwise velocity fields are depicted at the centre plane of the models for all three cases. Interpolation of data from nine *XZ*

planes resulted in the spanwise cross sections of the streamwise velocity flow field immediately downstream of the rear wheel of the leading rider. Due to the presence of the trailing cyclist, at Spacing 1 there is only a small region where a complete cross section is possible between the leading-rider rear wheel and trailing-rider front wheel. There is negligible difference in the streamwise velocity fields when comparing the wake of the single rider and the leading rider for the largest spacing tested. This indicates that the trailing rider has negligible forward influence on the leading rider at this separation distance. This is consistent with previous observations of drag that show negligible change in force for the leading rider with a second rider at one bicycle length separation [8].

For the minimum spacing there is an increase in the velocity deficit, predominantly in the centre of the wake, compared to the single or Spacing 2 cases. Differences in velocity between cases have been quantified by averaging streamwise velocity over the interrogation region. Normalised velocity for the single rider and tandem riders at Spacing 1 and Spacing 2 were 0.76, 0.73 and 0.76 respectively. This confirms that the overall velocity difference between the single rider and the leader at Spacing 2 is negligible. However, at minimum separation (Spacing 1) the velocity deficit across the leader is greater than for a single rider, despite having lower drag.

The small difference in streamwise velocity between the single rider case and that for Spacing 2 is consistent with force results, which have reported negligible drag reduction for the leading rider at a separation distance of one bicycle length [8]. At Spacing 1 the leading rider in a tandem pair has been shown to experience a small drag reduction of the order of 5% [8]. The field-averaged velocity shows a decrease in velocity of the wake of the leader at Spacing 1, which indicates greater energy loss compared to the single cyclist. Greater losses in the wake suggest an increase in drag, rather than the decrease measured in force tests. In fact, this reduction in velocity is likely due to forward interference from the trailing rider. Numerical modelling by Blocken *et al.* [12] have shown that the presence of the trailing rider acts to increase pressure on the rear of the leading cyclist. Assuming constant total pressure, this would correspond with reduced local velocity, as seen in the velocity profiles. It is this base pressure increase that is seen to be responsible for the leading-cyclist drag reduction. However, PIV results do not provide pressure data so this cannot be confirmed from these results.

Conclusion

In this study experiments utilising two-dimensional PIV in a water channel with scaled models have demonstrated the ability to gain information of the flow field around cyclists that has previously been difficult to obtain using real athletes and intrusive measurement techniques in a wind tunnel. High-resolution PIV velocity fields of a 1:4.5 scale model were compared with similar measurements obtained in a wind tunnel using a full-scale mannequin pedalling at realistic elite-level cadences and riding speeds. Despite the order-of-magnitude Reynolds number difference and some variations in the geometry of the models (body/bicycle), good agreement between the flow fields was observed for both quasi-steady and pedalling conditions. This was shown for both symmetric and asymmetric flow states, and highlights the robustness and Reynolds number insensitivity in the formation of the primary wake structures. In addition, water channel experiments with two drafting model cyclists showed that there was negligible influence on the near wake shed from the leading rider for separations greater than a bicycle length.

References

[1] Kyle, C.R. and Burke, E.R., Improving the racing bicycle, *Mechanical Engineering*, **106(9)**, 1984, 34–45.

[2] Grappe, F., Candau, R., Belli, A. and Jean Denis, R., Aerodynamic drag in field cycling with special reference to the Obree's position, *Ergonomics*, **40(12)**, 1997, 1299–1311.

[3] Jeukendrup, A.E., and Martin, J., Improving cycling performance: how should we spend our time and money, *Sports Medicine*, **31(7)**, 2001, 559–569.

[4] Zdravkovich, M., Achcroft, M., Chrisholm, S., and Hicks, N., Effect of cyclists posture and vicinity of another cyclist on aerpdynamic drag, *The Engineering of Sport*, **1**, 1996, 21–28.

[5] Crouch, T.N., Burton, D., Brown, N.A.T., Thompson, M.C., and Sheridan, J., Flow topology in the wake of a cyclist and its effect on aerodynamic drag, *Journal of Fluid Mechanics*, **748**, 2014, 5–35.

[6] Griffith, M.D., Crouch, T.N., Thompson, M.C., Burton, D., Sheridan, J. and Brown, N.A.T., Computational Fluid Dynamics Study of the Effect of Leg Position on Cyclist Aerodynamic Drag, *Journal of Fluids Engineering*, **136(10)**, 2014, 101105.

[7] Kyle, C.R., Reduction of wind resistance and power output of racing cyclists and runners travelling in groups, *Ergonomics*, **22(4)**, 1979, 387–397.

[8] Barry, N., Sheridan, J., Burton, D., and Brown, N.A.T., The effect of spatial position on the aerodynamic interactions between cyclists, *Procedia Engineering*, **72**, 2014, 774–779.

[9] Fouras, A., Lo Jacono, D., and Hourigan, K., Targetfree Stereo PIV: a novel technique with inherent error estimation and improved accuracy, *Experiments in Fluids*, **44(2)**, 2007, 317–329.

[10] Crouch, T.N., Burton, D., Thompson, M.C., Martin, D.T., Brown, N.A.T., and Sheridan, J., A Phase-Averaged Analysis of the Pedalling Cyclist Wake, Proceedings of the 19th Australasian Fluid Mechanics Conference, Melbourne, Victoria, Australia, 2014.

[11] Zhou, J., Adrian, R., Balachandar, S., and Kendall, T., Mechanisms for generating coherent packets of hairpin vortices in channel flow, *Journal of Fluid Mechanics*, **387**, 1999, 353–396.

[12] Blocken, B., Defraeye, T., Koninckx, E., Carmeliet, J., and Peter, H., CFD simulations of the aerodynamic drag of two drafting cyclists, *Computers & Fluids*, **71**, 2013, 435–445.